

Suppression of Notch Signaling in Osteoclasts Improves Bone Regeneration and Healing

Peeyush N. Goel,^{1,2} Yasaman Moharrer,^{1,2} John H. Hebb,^{1,2,3} Alexander J. Egol,^{1,2} Gurpreet Kaur,⁴ Kurt D. Hankenson,⁵ Jaimo Ahn,^{1,2} Jason W. Ashley⁶

¹Department of Orthopaedic Surgery, Perelman School of Medicine, University of Pennsylvania, Philadelphia, Pennsylvania, ²Translational Musculoskeletal Research Center, Corporal Michael J. Crescenz VA Medical Center, Philadelphia, Pennsylvania, ³Georgetown University School of Medicine, Washington, District of Columbia, ⁴Department of Biological Sciences, University of the Sciences, Philadelphia, Pennsylvania, ⁵Department of Orthopaedic Surgery, University of Michigan, Ann Arbor, Michigan, ⁶Department of Biology, Eastern Washington University, Cheney, Washington

Received 15 February 2019; accepted 28 May 2019

Published online in Wiley Online Library (wileyonlinelibrary.com). DOI 10.1002/jor.24384

ABSTRACT: Owing to the central role of osteoclasts in bone physiology and remodeling, manipulation of their maturation process provides a potential therapeutic strategy for treating bone diseases. To investigate this, we genetically inhibited the Notch signaling pathway in the myeloid lineage, which includes osteoclast precursors, using a dominant negative form of MAML (dnMAML) that inhibits the transcriptional complex required for downstream Notch signaling. Osteoclasts derived from dnMAML mice showed no significant differences in early osteoclastic gene expression compared to the wild type. Further, these demonstrated significantly lowered resorption activity using bone surfaces while retaining their osteoblast stimulating ability using *ex vivo* techniques. Using *in vivo* approaches, we detected significantly higher bone formation rates and osteoblast gene expression in dnMAML cohorts. Further, these mice exhibited increased bone/tissue mineral density compared to wild type and larger bony calluses in later stages of fracture healing. These observations suggest that therapeutic suppression of osteoclast Notch signaling could reduce, but not eliminate, osteoclastic resorption without suppression of restorative bone remodeling and, therefore, presents a balanced paradigm for increasing bone formation, regeneration, and healing. © 2019 Orthopaedic Research Society. Published by Wiley Periodicals, Inc. *J Orthop Res* 37:2089–2103, 2019

Keywords: Notch signaling; osteoclasts; osteoblasts; bone formation; regeneration; fracture healing

Fracture healing is a complex multi-phase process. At the early stage of healing, osteoclasts remodel the fracture margin in preparation for callus formation.^{1–3} As the initially cartilaginous soft callus calcifies into a fracture-stabilizing bony callus, osteoclasts return, and alongside osteoblasts, remodel the callus until physiological bone architecture is restored. Should fracture healing proceed inefficiently, however, the discontinuity caused by the fracture may persist or, following apparent healing, there may be persistent structural weakness that can contribute to re-fracture.^{4,5} This is of concern in aged individuals, where the efficiency of the bone healing process is diminished. Current strategies to improve skeletal healing include local surgical delivery of osteo-inductive materials or proteins and systemic delivery of anti-resorptive or anabolic therapy.⁶ However, none of these therapies accelerate normal fracture healing nor are they recommended for long-term use as re-fracture preventatives.^{7–9} New approaches based on a clear mechanistic understanding of bone biology and regeneration represent opportunities to address these limitations.

Bone resorbing osteoclasts are formed from hematopoietic progenitors of the monocyte/macrophage lineage in a multi-step process, which includes progenitor proliferation, expression of functional genes, and fusion into mature, resorption-capable giant cells.^{10,11} In addition to their role as bone resorbing cells, osteoclasts promote the differentiation of bone-forming osteoblasts.^{12–15} This coupling role is apparent in both genetic and pharmacologic suppression of osteoclast numbers, which result in a coupled reduction in osteoblasts.^{12,13} Conversely, approaches that inhibit osteoclast activity while preserving osteoclast number preserve osteoblast function.¹⁶ Thus, understanding of mechanisms of osteoclast function (as opposed to those of initial differentiation or survival) are of interest, as inhibition of osteoclast maturation may reduce resorption while preserving osteoblast activity and physiological remodeling.

One such osteoclast maturation-controlling system is Notch signaling. We, along with other research groups, have demonstrated that Notch signaling plays a bi-phasic role in osteoclastogenesis, in which, prior to commitment, stimulation of Notch signaling inhibits osteoclast differentiation. After commitment with receptor activator of nuclear factor κ -B ligand (RANKL), however, Notch signaling is required for final maturation and full functionality.^{17–21} Notch signaling is initiated by binding of one of five ligands to one of four Notch receptors. This binding releases the intracellular portion of the receptor (NICD), which translocates to the nucleus and binds recombination signal binding protein for immunoglobulin kappa J region

Conflicts of interest: None.

This work was performed at VA Medical Centre, Philadelphia and School of Veterinary Medicine, Hill Pavilion at University of Pennsylvania. Grant sponsor: AO Foundation (J.W.A.); Grant number: S-16-12A; Grant sponsor: NIH/NIAMS; Grant number: P30AR069619.

Correspondence to: Jaimo Ahn (T: 215-662-3340; F: 215-349-5890; E-mail: jaimo.ahn@uphs.upenn.edu); Jason Waid Ashley (T: 509-359-4665; F: 509-359-6867; E-mail: jashley6@ewu.edu)

© 2019 Orthopaedic Research Society. Published by Wiley Periodicals, Inc.

(RBPJ κ), a transcriptional regulator, to displace co-repressors and recruit co-activators. Mastermind-like (MAML) is a crucial transcriptional co-activator that serves as an interface between NICD and RBPJ κ .^{22–24} In the present study, inhibition of Notch signaling was achieved via expression of dnMAML, which competitively inhibits transcription complex formation by binding NICD and RBPJ κ , but no other co-activators (Fig. 1A).^{22,25} dnMAML was expressed in the myeloid lineage, which includes osteoclasts and their precursors, via a cross between Rosa-dnMAML mice, which carry a LoxP-STOP-LoxP-dnMAML expression cassette, and mice that express Cre recombinase under the control of the lysozyme M (LysM), promoter.

We asked, (i) is osteoclast Notch signaling required for bone remodeling and architecture at physiological baseline, and (ii) will inhibition of osteoclast Notch signaling improve fracture healing?

METHODS AND MATERIALS

Mice Breeding

Experimental mice cohorts were generated by mating homozygous LysM^{Cre/Cre} (B6.129P2-Lyz2^{tm1(cre)If0}/J; Jackson Labs, Bar Harbor, ME) with heterozygous Rosa^{fl-STOP-fl-dnMAML/+} mice (C57/Bl6 genetic background). The genotypes of the offspring obtained were LysM^{Cre/+}/Rosa^{fl-STOP-fl-dnMAML/+} (dnMAML mice) and LysM^{Cre/+}/Rosa^{+/+} (control or WT) (Fig. 1B). The LysM-Cre²⁶ mouse has been used previously in multiple studies to investigate the roles of specific molecules in osteoclast differentiation without confounding effects during embryonic development.^{27–29}

Osteoclast Culture and Maintenance

Osteoclast precursors were cultured and differentiated as previously described.^{21,30} Briefly, bone marrow from femurs and tibias were flushed using α -minimum essential medium (α -MEM) and centrifuged. Cells were later incubated overnight to allow adherent cells to attach to the plate. Next day, non-adherent cells were transferred to new plates with 35 ng/ml recombinant mouse monocyte/macrophage colony-stimulating factor (MCSF) (BioLegend, San Diego, CA). Upon 70% confluency, adherent osteoclast precursors were harvested using Accutase and later seeded at a density of approximately 26,000 cells per cm² in α -MEM with 35 ng/ml MCSF and 100 ng/ml recombinant mouse RANKL (Shenanandoah Biotechnology, Warwick, PA). Differentiation medium was replaced every other day. After a period of 3–4 days, osteoclastogenesis was completed and multinuclear cells were observed. The osteoclasts were later tartrate-resistant acid phosphatase (TRAP) stained according to the kit instructions (Sigma-Aldrich, St. Louis, MO) to evaluate the enzymatic activity or lysed for RNA extraction.

Fluorescence Microscopy

Osteoclasts were differentiated on cover glass circles #1.5, 12 mm (Electron Microscopy Sciences, Hatfield, PA) and placed into 24-well plates. After a period of 4 days, cells were fixed using 4% paraformaldehyde for 10 min at room temperature (RT) and washed with phosphate-buffered saline (PBS) twice. 0.1% Triton X-100 was added for 5 min with subsequent washing using PBS. Cells were then blocked in 1% bovine serum albumin for 30 min and stained using Alexa Fluor 594

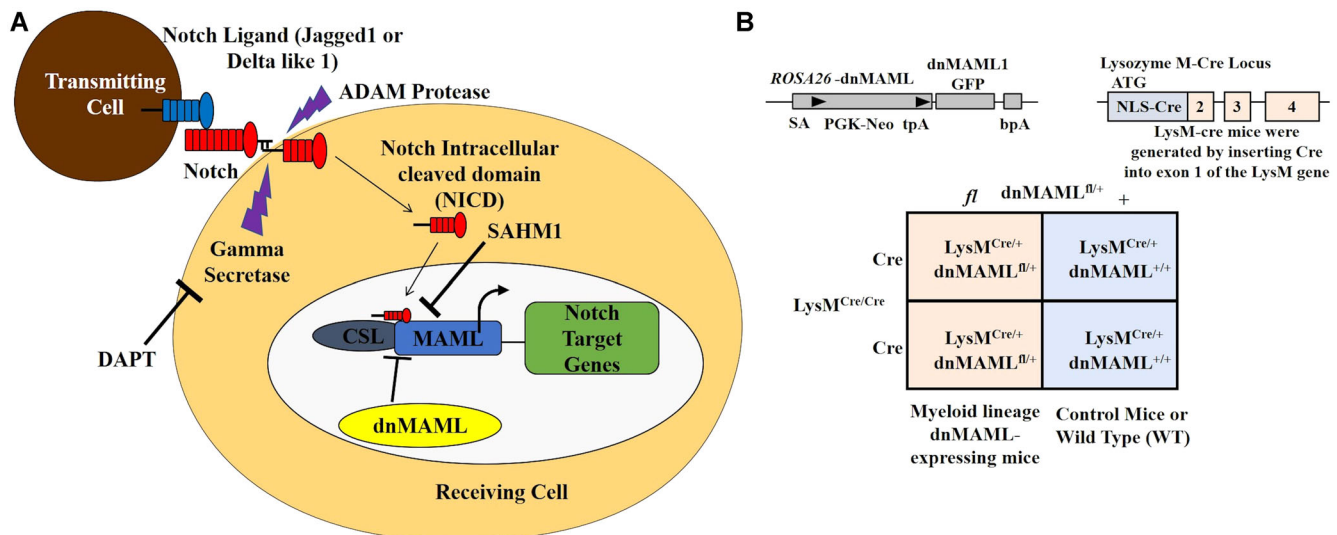


Figure 1. Genetic manipulation of Notch signaling in osteoclasts. (A) Trans-activation of Notch signaling in the receiving cell is initiated via interaction between Notch receptor and ligand (Jagged1 or Delta-like1) presented by the transmitting cell. This initiates proteolytic cleavage events that release the Notch intracellular domain (NICD) that translocates to the nucleus and forms a transcriptional complex with MAML and CSL. Notch signaling can be inhibited at the receptor level with DAPT, a γ -secretase inhibitor that inhibits NICD release, or at the transcriptional level by either expressing dominant negative MAML (dnMAML) or treating with SAHMI, a peptide dnMAML mimetic. (B) In this study, we inhibited Notch signaling in osteoclast precursors via Lysozyme M promoter-driven dnMAML expression. Mice with genotypes LysM-Cre⁻ dnMAML^{-/-} (WT) and LysM-Cre⁻ dnMAML^{Mye+/-} (dnMAML) were utilized for subsequent studies. CSL, CBF1/Suppressor of Hairless/LAG-1. [Color figure can be viewed at wileyonlinelibrary.com]

labeled Phalloidin (Molecular Probes, Eugene, OR) with 5 µl in 200 µl PBS/well. The samples were incubated for 30 min in dark. Cells were washed using PBS and then coverslips mounted on clear glass slides after addition of Prolong Gold antifade reagent with 4',6-diamidino-2-phenylindole (Thermo Fisher Scientific, Waltham, MA). Finally, the coverslips were sealed using nail paint and Images were acquired using a Nikon Eclipse fluorescence microscope (Nikon, Melville, NY).

RNA Isolation and Quantitative Polymerase Chain Reaction (PCR)

RNA was extracted using TRIzol from Thermo Fisher Scientific as per the manufacturer's instructions.²¹ RNA concentration was determined using a spectrophotometer and 1 µg of RNA was used as starting material for complementary DNA (cDNA) preparation. Total RNA was reverse transcribed using SuperScript VILO (Thermo Fisher Scientific). cDNA was then used as a template for amplification using SYBR Green in a ViiA7 Real time PCR system (Thermo Fisher Scientific). Each of the samples were set up in triplicates and the experiments were repeated at least thrice for data integrity and accuracy. Gene expression was normalized to 18S. The list of primers is provided in Table 1.

Jagged 1 Stimulation and Hes1 Expression

Notch signaling was stimulated using immobilized Jagged1 as previously described.^{21,30} Goat immunoglobulin G (Jackson Immunology, West Grove, PA) and Jagged-1, a Notch ligand (R&D Systems, Minneapolis, MN) were made in PBS at a concentration of 10 µg/ml and added to 48-well plates. Wells were then washed using PBS and later 26,000 osteoclast precursors were seeded (24 h pre-exposure to either MCSF alone or both MCSF and RANKL). Plates were incubated for at least 24 h prior to harvesting the cells for RNA extraction and analysis of Hes1 gene expression.

Mineral Dissolution Assay

Nearly, 50,000 cells were seeded into a 24-well Osteo-assay plate (Corning Life Sciences, Tewksbury, MA) coated with calcium phosphate. Both WT and dnMAML osteoclast precursors were seeded and later treated with MCSF or MCSF and RANKL for a total of 5 days. Media were replenished alternatively as described earlier. The remaining mineral was Von Kossa stained as per the protocol described.²¹ Cells were washed with PBS and incubated in 10% bleach for 5 min followed by washing twice with deionized water. Three hundred microliters of 5% silver nitrate was added to the plate and incubated at RT for 30 min. Wells were then washed thoroughly using deionized water. Later, 300 µl of 5% sodium carbonate made in formalin was added and incubated for another 5 min at RT. Finally, the solution was removed from the wells and air dried. Plates were then scanned and quantified using ImageJ software (NIH, Bethesda, MD).

Pit Formation Assay and Determination of TRAP Activity

Cortical bone slices (Immunodiagnostic Systems, East Boldon, UK) were purchased for in vitro assessment of osteoclastic bone resorption using pit formation assay as per the procedure described with slight modifications.³¹⁻³³ Bone chips were sterilized under ultraviolet for at least 2 h and then washed with media before placing in 96-well plates. Twenty thousand cells per two hundred microliter of (WT and dnMAML) were seeded onto the bone slices containing either MCSF or MCSF and RANKL for a total of 12 days. Conditioned media was collected and replenished with new media every third day. The former was then stored at -20°C for further analysis of TRAP and type I collagen C-telopeptide (CTX-1) levels. At day 12th, osteoclasts were removed, and slices were stained with 1% toluidine blue in 1% sodium borate solution. Bone slices were dried and imaged using Nikon Eclipse light microscope. Pits were counted and measured using ImageJ software. TRAP/TRACP activity was determined^{34,35} using TRAP solution buffer consisting of L-

Table 1. List of Primers Used for Semiquantitative Reverse Transcription Polymerase Chain Reaction

Sl. No.	Name	Forward	Reverse
1	TRAP/ACP5	CAGCTCAGTTGGGTAGCACA	AGCCACAAATCTCAGGGTGG
2	CSTK	CAGTGTGGTGGTGGGCTAT	CATGTTGGTAATGCCGCAGG
3	MMP9	CAGACGTGGGTCGATTCCAA	TCATCGATCATGTCCTCGCGG
4	Wnt10b	ACCACGACATGGACTTCGGAGA	CCGCTTCAGGTTTTCCGTTACC
5	Hes1	GAGGCTGCCAAGGTTTTTGG	ACTTTACGGGTAGCAGTGGC
6	ALP	CCAGAAAGACACCTTGACTGTGG	TCTTGTCCGTGTCGCTCACCAT
7	OSX	ATGGCGTCCTCTCTGCTTGA	TTCCCAGGGTTGTTGAGTC
8	OCN	GCAATAAGGTAGTGAACAGACTCC	CCATAGATGCGTTTTGTAGGCCG
9	Runx2	CCTGAACTCTGCACCAAGTCCT	TCATCTGGCTCAGATAGGAGGG
10	DC-STAMP	TTTGCCGCTGTGGACTATCTGC	GCAGAATCATGGACGACTCCTTG
11	OC-STAMP	GGCTCAGAAGTTACCCACTGTC	GGAGGTTGGTTGAGGACGAAGA
12	MAML	CCAGCTTTGATGGCATATCTTCC	CTACAGGGACACTGGAAGGGTT
13	18S	GGTAACCCGTTGAACCCCAT	CAACGCAAGCTTATGACCCG

ascorbic acid, di-sodium tartrate, 4-nitrophenylphosphate, and reaction buffer (1 M acetate, 0.5% Triton X-100, 1 M NaCl, 10 mM ethylenediaminetetraacetic acid pH = 5.5). Ten microliters of condition medium was dispensed into a new 96-well plate and 90 μ l TRAP solution buffer was added. The mix was incubated at 37°C for about 15 min in the dark. The reaction was stopped using 0.3 N NaOH, and absorbance was measured at 405 nm using a BioTek spectrophotometer (BioTek, Winooski, VT).

Determination of CTX-1 and Osteocalcin Levels

CTX-1 levels were measured in serum collected from 3-month-old female and male (WT and dnMAML mice) and conditioned medium collected from bone slices using CTX-I detection enzyme-linked immunosorbent assay (ELISA) kit (Chondrex, Inc., Redmond, WA). It is based on a competitive assay system with a monoclonal antibody, which recognizes conserved peptide sequences in mouse.³⁶ Levels of osteocalcin, a bone formation marker³⁷ was evaluated using mouse osteocalcin ELISA (NBP2-68151; Novus Biologicals, Centennial, CO) in serum collected from 3-month old WT and dnMAML mice, respectively, as per the instructions provided in the kit.

Osteoblast Culture Maintenance, Alkaline Phosphatase (ALP) Activity, and Alizarin Staining

Adherent bone marrow stromal cells were cultured to 70% confluency. Cells were then harvested and then seeded at a density of 30,000 cells per cm². WT cells were maintained in maintenance media (α -MEM supplemented with 10% fetal bovine serum, 1% penicillin-streptomycin, 1% L-glutamine, 1% non-essential amino acids), osteogenic media (maintenance media + 10 mM β -glycerol phosphate + 50 μ M ascorbate-2-phosphate + 100 nM dexamethasone), osteogenic media in combination with conditioned media collected from either WT or dnMAML osteoclasts (here condition media was first concentrated using 3 kDa cut off concentration filters (Millipore, Burlington, MA) and then mixed in a ratio of 1:10 with osteogenic media), or osteogenic media in combination with 30 ng/ml bone morphogenetic protein 6 (BMP-6) (R&D Systems). Media were refreshed every third day. ALP activity was measured by SensoLyte pNPP Alkaline Phosphatase Assay Kit (AnaSpec, Inc., Fremont, CA)³⁸ as per the manufacturer's instructions. Mineralized nodules were stained with alizarin red as per the protocol described earlier.³⁹

Skeletal Phenotyping

WT and dnMAML mice were given a subcutaneous injection of calcein and alizarin red to label bone mineralizing surfaces fluorescent green and red (9 and 2 days prior to euthanasia). Following euthanasia, right femurs were fixed, decalcified, and sectioned. Paraffin sections were TRAP-stained for quantification of osteoclast numbers. Left femurs were fixed,

embedded in polymethylmethacrylate, sectioned, and stained using trichrome^{40,41} for quantification of osteoblasts per trabecular area and osteoblast surface per bone surface. Unstained sections were imaged fluorescently for quantification of mineralizing surfaces and determination of bone formation rate. Images were acquired using a Nikon Eclipse fluorescence microscope and analyzed using Osteomeasure software (OsteoMetrics, Atlanta, GA). Left tibias were fixed and analyzed via μ CT with subsequent mechanical testing. RNA was extracted from right tibias for analysis of osteoclast (TRAP, CSTK, MMP9, and Wnt10B) and osteoblast gene expression (ALP, Osterix, Osteocalcin, and Runx2), respectively.

Fracture Protocol and Surgery

Mice were fractured as per the protocol described earlier.⁴² Briefly, a small incision was created around the mouse's knee and a 27-gauge needle was placed in the tibial tuberosity just above the patella for fracture stabilization. Following pinning and incision, a traumatic 3-point-bend fracture was generated using a modified guillotine (consists of a weight [220 g] sitting 7 cm above the metal lever). The setup of fracture device is outlined in Figure S1. Mice were recovered from anesthesia on a warm water pad and received a subcutaneous dose of extended release buprenorphine (0.5 mg/kg) after the surgery, and then once every third day. Animals were humanely euthanized for analysis at 10-, 20-, and 40-days post fracture (DPF). Fracture calluses were analyzed using μ CT and histology.

MicroCT (μ CT) Parameters⁴³⁻⁴⁶

Samples were imaged in a μ CT scanner (model μ CT50; Scanco Medical, Wangen-Brüttisellen, Switzerland). A Gaussian low-pass filter ($\sigma = 0.8$, support = 1) was used for all analyses. Trabecular bone parameters were measured by analyzing 150 slices of the distal metaphysis. Cortical bone parameters were measured by analyzing 50 slices in the mid-diaphysis. A semi-automated contouring method was used to determine the outer cortical bone perimeter. The distal metaphyseal regions were used for evaluation of bone volume, total volume, bone volume/total volume, trabecular number, trabecular thickness, trabecular spacing, bone mineral density, and tissue mineral density while mid-diaphyseal regions for determining cortical thickness, cortical bone mineral density, and cortical tissue mineral density. Fractured tibias were quantified based on region of interest of each callus and the following parameters were determined: mineralized callus volume (BV), total callus volume (TV), mineralized callus volume fraction (BV/TV), bone mineral density (BMD), tissue mineral density (TMD), and average callus area. The latter was calculated by counting the number of slices multiplied by the size of the slice (0.006 mm/slice) to obtain the total length of the callus, and subsequently, average callus area was determined by dividing bone volume to total callus length.

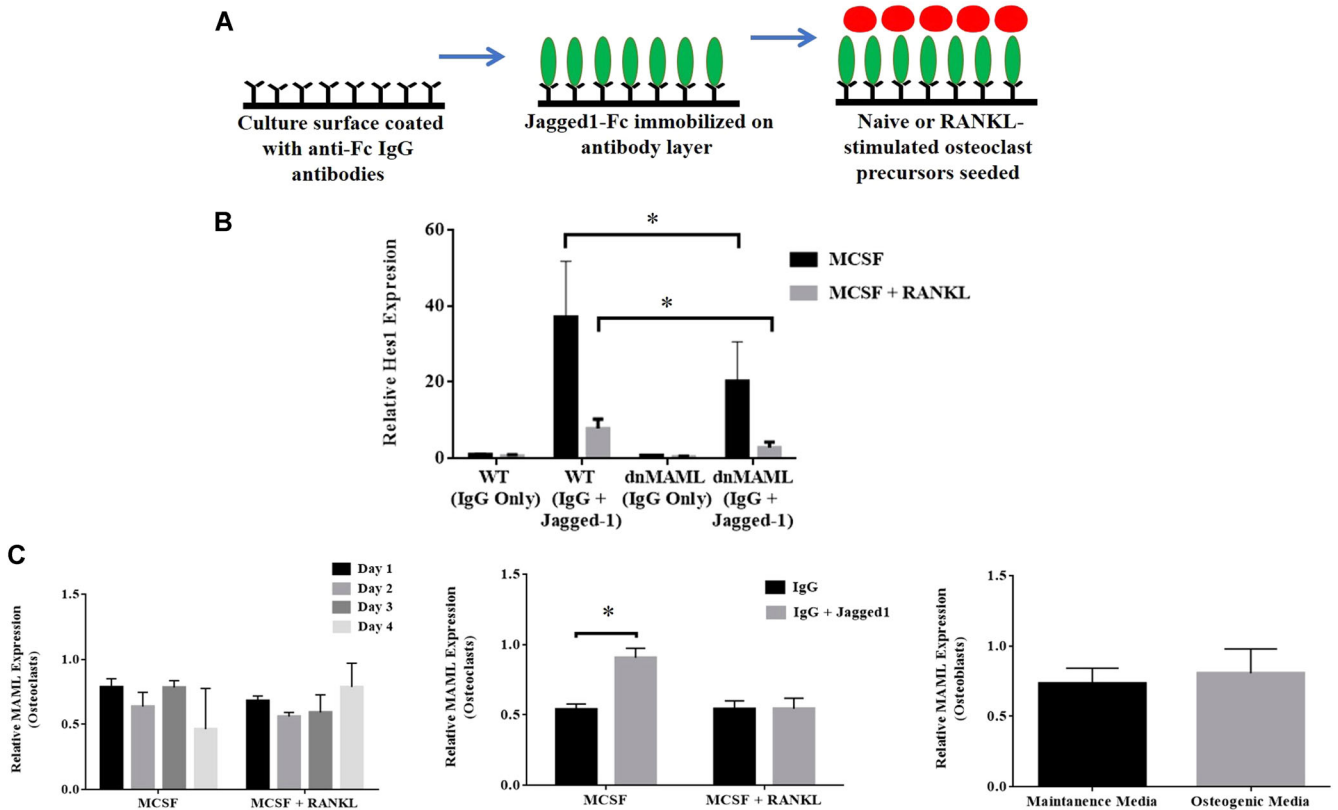


Figure 2. dnMAML suppresses Jagged1 induction of Hes1. Ex vivo generated osteoclasts from both WT and dnMAML mice were subjected to Notch signaling stimulation via Jagged1 following culture with macrophage colony-stimulating factor (MCSF) alone or MCSF + RANKL. After 24 h of Jagged1 stimulus, relative expression of Hes1 was determined via quantitative reverse transcription polymerase chain reaction (qRT-PCR). (A) Schematic representation of Notch signaling stimulation via immobilized Jagged1. (B) Relative expression of Hes1 (Notch target gene) following exposure to Jagged1 or immunoglobulin G (IgG) demonstrated that Jagged1 stimulation produced a robust increase in Hes1 expression that was blunted by dnMAML. MCSF + RANKL treatment also reduced Jagged1-stimulated Hes1 expression. (C) MAML gene expression analysis in osteoclasts and osteoblasts was performed using qRT-PCR. Relative levels of MAML were unchanged during the differentiation process for both the cell types. Jagged1 treatment, however, significantly increased MAML expression in osteoclast precursors maintained with MCSF, but not MCSF + RANKL. Values represented are mean \pm SD from at least three independent experiments. *p* value was calculated using Student *t* test (**p* < 0.05). [Color figure can be viewed at wileyonlinelibrary.com]

Mechanical Testing

Following μ CT, tibias were placed on the fixed supports of 3-point bending fixture (14 mm span). The actuator of testing system (DaynaMight; Instron Corp., Norwood, MA) was centered above the medial region and anterior sides facing forward and down, respectively. To keep the bone in place a pre-load of 2 N was applied. A load at constant rate of 0.005 mm/s was applied centrally until failure occurred. The force–displacement curve was then recorded for each sample and the structural stiffness determined by measuring the slope of curve at its linear portion. Additionally, ultimate force (force at failure) was determined.

Histological Parameters

Femurs from the skeletal phenotyping group were paraffin-embedded and sectioned for TRAP staining. Fracture callus sections were TRAP-stained for quantification of osteoclast numbers and Safranin O stained for quantification of callus area and cartilage area. TRAP staining was performed as per the protocol from University of Rochester. Paraffin sections were first deparaffinized

using xylene and rehydrated through graded ethanol (100%, 95%, and 80%) to distilled water. Slides were then placed in pre-warmed TRAP staining solution mix (sodium acetate, tartaric acid, glacial acetic acid, fast Red violet, and naphthol) for about an hour and rinsed in distilled water. Slides were later counterstained with 0.02% Fast Green for 45 s and rinsed quickly in distilled water followed by dehydration using ethanol (80%, 95%, and 100%) with clearing in xylene. Slides were mounted using Permunt (Thermo Fisher Scientific) and imaged using Nikon Eclipse light microscope. Osteoclasts were counted using the Osteomeasure software. Safranin O staining was performed as per the protocol described earlier^{47–49} and from IHC world. Briefly, sections were deparaffinized and hydrated. Slides were stained using Weigert's iron hematoxylin working solution, washed, and then counterstained using fast green. Slides were rinsed quickly in 1% acetic acid and then stained using 0.1% Safranin O solution. Finally, the slides were dehydrated and mounted as described above. Slides were imaged using Nikon Eclipse light microscope. Cartilage and callus area were determined using the Osteomeasure software.

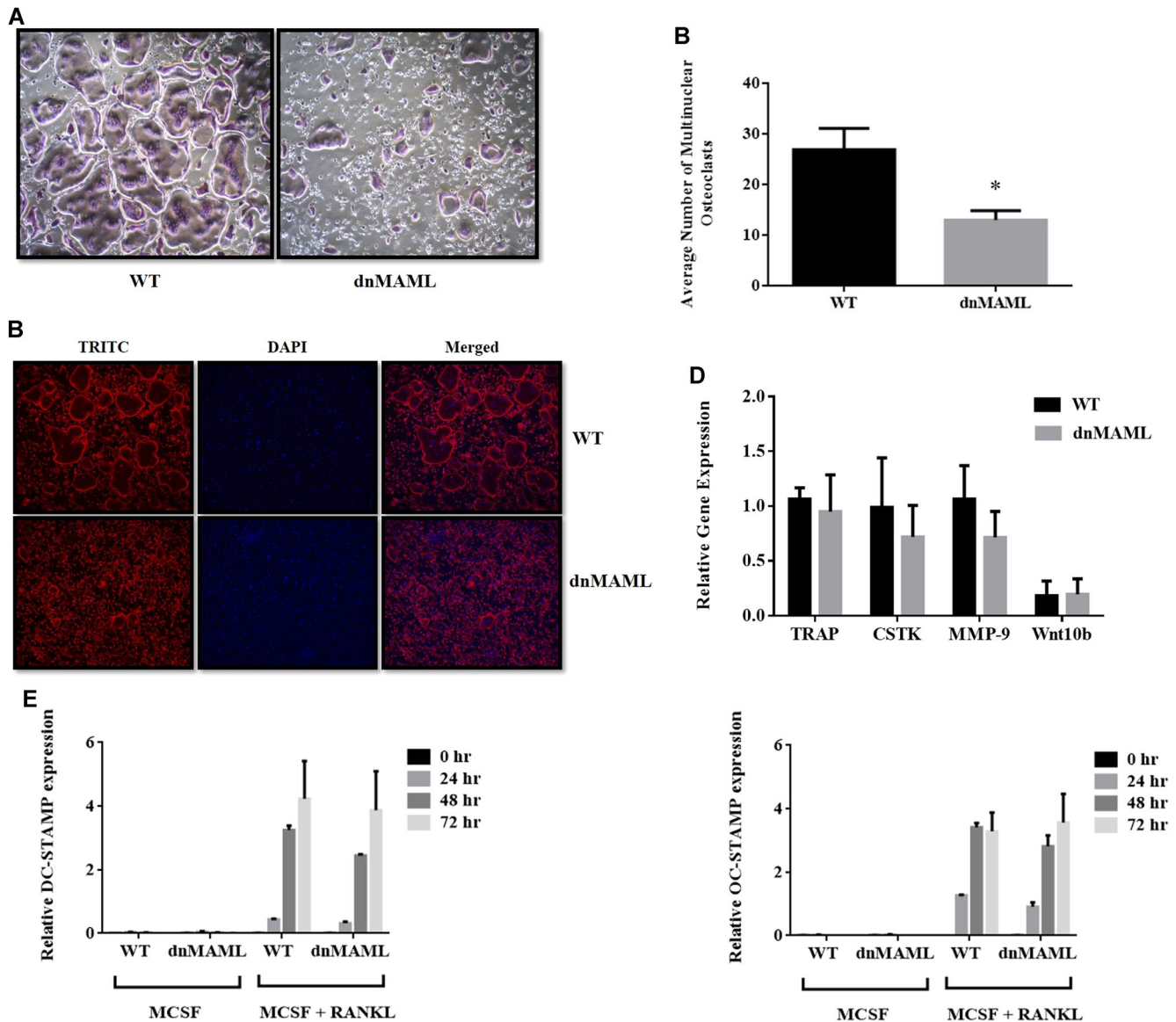


Figure 3. Genetic inhibition of Notch signaling suppresses osteoclast maturation but does not impact early gene expression. Bone marrow-derived macrophages were collected from both wild-type (WT) and dnMAML mice and differentiated into osteoclasts ex vivo. (A) Tartrate-resistant acid phosphatase (TRAP)-stained osteoclasts (purple) in WT group were giant and well-fused while osteoclasts from Notch-inhibited mice failed to fuse effectively and remained immature. (B) Quantification of TRAP-stained multinuclear osteoclasts showed a significant reduction in average number of osteoclasts in dnMAML group. (C) To delineate cytoskeletal reorganization, actin filaments were assessed using Phalloidin staining. There were fewer and smaller osteoclasts in dnMAML group, but these cells still demonstrated podosome belts, suggesting normal actin organization. (D) and (E) Expression analysis of osteoclastic marker genes (TRAP, cathepsin K [CTSK], matrix metalloproteinase 9 [MMP9], and Wnt10b) and osteoclast-specific fusion markers dendritic cell-specific transmembrane protein and osteoclast stimulatory transmembrane protein (DC-STAMP and OC-STAMP) ex vivo showed no significant differences between the dnMAML and WT groups. Values represented are mean \pm SD from at least three independent experiments. *p* value was calculated using Student *t* test ($*p < 0.05$). [Color figure can be viewed at wileyonlinelibrary.com]

Biological Variables and Data Analysis

Experiments were carried out in both male and female animals as skeletal problems, fractures, and healing issues affect both sexes. Skeletal phenotyping was performed in both 3- and 6-month males and female C57/BL6 mice cohorts whereas fractures and other ex vivo work in 3-month male and female mice (WT and dnMAML).

Statistics

All experiments were performed at least thrice independently and represented as mean \pm SD. Student *t* test was used for statistical analysis and *p* < 0.05 was considered statistically significant. Graphpad Prism 6.0 software (GraphPad, San Diego, CA) was used for graphical representation of the data. To increase rigor, analyses subject to

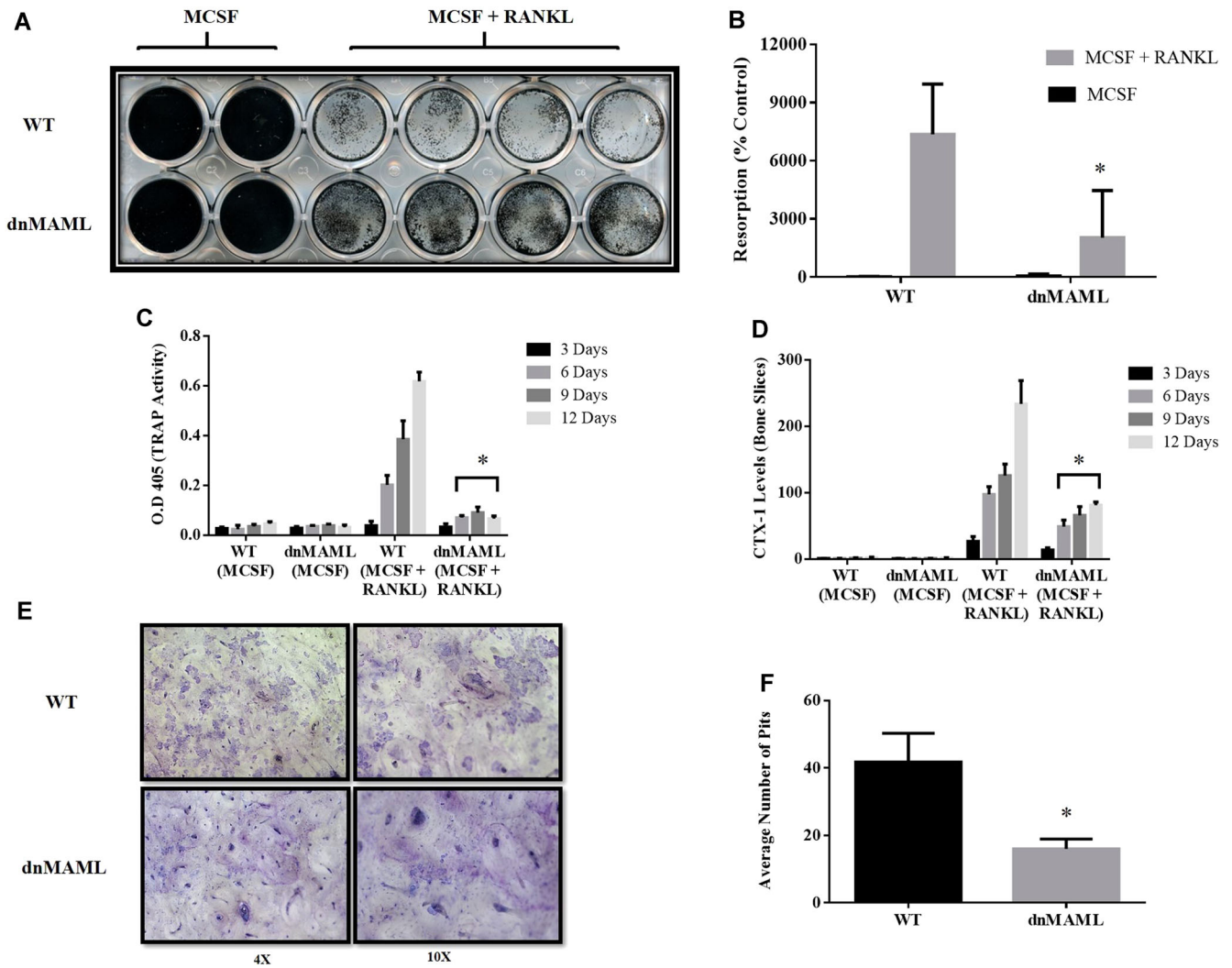


Figure 4. Genetic inhibition of Notch signaling reduces osteoclast resorptive function. (A) Osteoclast precursors generated ex vivo from both wild-type (WT) and dnMAML mice were differentiated and cultured on calcium phosphate coated surfaces for a period of 5 days. Following culture, osteoclasts were removed and the remaining minerals were von Kossa stained and (B) quantified using ImageJ software. dnMAML osteoclasts demonstrated significantly reduced resorptive activity compared with WT. (C) Osteoclast precursors were seeded on bovine cortical bone slices in 96-well plates and cultured in the presence of macrophage colony-stimulating factor (MCSF) alone or MCSF + RANKL for a period of 2 weeks. Conditioned media were collected every third day and tartrate-resistant acid phosphatase (TRAP) enzymatic activity was evaluated using pNPP chromogenic substrate. There was a significant reduction in TRAP activity in the conditioned media of dnMAML osteoclasts cultured with MCSF + RANKL on days 6, 9, and 12. (D) CTX-1, c-terminal fragments of type I collagen, levels were determined in condition media from WT and dnMAML osteoclasts. CTX-1 levels were significantly reduced in dnMAML osteoclasts cultured with MCSF + RANKL on days 6, 9, and 12. (E) At the conclusion of culture, bone slices were toluidine blue stained to reveal the resorption pits. (F) Quantification showed a significant reduction in number of resorption pits from dnMAML osteoclast cultures. Values represented are mean \pm SD from at least three independent experiments. *p* value was calculated using Student *t* test ($*p < 0.05$). [Color figure can be viewed at wileyonlinelibrary.com]

measurement variability (e.g., qPCR, ex vivo cellular assays, serum measurements) were performed in triplicate and those subject to evaluator variability (e.g., histomorphometry analysis) performed in a blinded fashion.

Study Approval

Mice were housed and procedures carried out in facilities provided by the University of Pennsylvania and the Philadelphia VA Medical Center both of which are AAALAC accredited. Procedures were approved by the

Institutional animal care and use Committee (IACUC) of the University of Pennsylvania.

RESULTS

dnMAML Suppresses Jagged1 Induction of Hes1 in Bone Marrow Macrophages and Pre-Osteoclasts

To assess the functionality of dnMAML in osteoclast precursors, cells from both WT and dnMAML mice were subjected to Notch signaling stimulation via immobilized Jagged1 after a 24-h pre-exposure to either MCSF alone or MCSF + RANKL (Fig. 2A). Twenty-four hours of Jagged1 stimulation produced

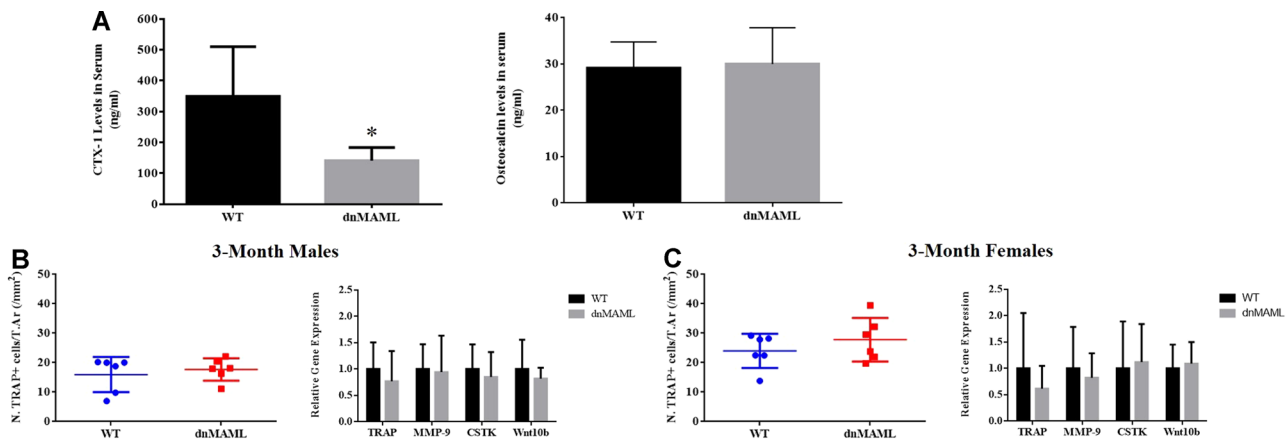


Figure 5. Notch inhibition impairs resorptive activity in vivo without impacting tartrate-resistant acid phosphatase (TRAP)⁺ cell numbers and gene expression profiles. (A) CTX-1 levels in serum obtained from 3-month-old male and female wild-type (WT) and dnMAML mice were significantly reduced in dnMAML mice suggesting reduced resorptive activity. No differences in serum osteocalcin (OCN) levels were observed between the two groups suggesting comparable osteoblast activity. TRAP⁺ cell numbers and expression profile of osteoclastic marker genes (TRAP, cathepsin K [CTSK], matrix metalloproteinase 9 [MMP9], and Wnt10b) were analyzed in (B) 3-month-old males and (C) 3-month-old females using TRAP staining and quantitative reverse transcription polymerase chain reaction (qRT-PCR), respectively. There were no significant differences in TRAP⁺ cell numbers or gene expression profiles between these groups. Values represented are mean \pm SD and *p* value was calculated using Student *t* test (**p* < 0.05). [Color figure can be viewed at wileyonlinelibrary.com]

a robust induction of Hes1, a Notch target gene, in both bone marrow macrophages and pre-osteoclasts, and this induction was blunted by the presence of dnMAML (Fig. 2B). Interestingly, prior stimulation of RANK signaling likewise reduced Hes1 transcription, and this effect was further diminished by the presence of dnMAML (Fig. 2B). We also estimated the levels of MAML during the differentiation of both osteoclasts and osteoblasts. Levels of MAML were relatively unaltered in both the osteoclasts and osteoblasts (Fig. 2C). However, we observed a significant difference in MAML expression levels upon stimulation with Jagged 1 in MCSF alone group whereas in MCSF + RANKL-treated osteoclasts the levels of MAML were unchanged (with or without Jagged 1 stimulation), as shown in Figure 2C.

Notch Signaling Is Not Required for Early Osteoclast Gene Expression

Osteoclasts derived from both WT and dnMAML mice were subjected to TRAP staining. Osteoclasts from WT were giant and fully mature while the osteoclasts from dnMAML mice failed to fuse effectively and remained immature (Fig. 3A). Further, the number of mature osteoclasts were significantly higher in the control group (Fig. 3B). dnMAML cells, nevertheless, remained TRAP-positive indicating a failure not in differentiation per se, but fusion and maturation. To delineate cytoskeletal reorganization and actin ring formation, actin filaments were stained with phalloidin. While dnMAML osteoclasts were smaller and fewer, those that did form demonstrated normal podosome belts (Fig. 3C). Gene expression analysis of early osteoclast marker genes (TRAP, cathepsin K [CTSK], matrix metalloproteinase 9 [MMP9], and Wnt10b) found no

significant difference between WT and dnMAML osteoclasts providing further evidence that Notch signaling drives maturation rather than initial differentiation of osteoclasts (Fig. 3D). The smaller and immature osteoclasts observed in dnMAML group indicated a possible defect in fusion process. To address this, we carried out gene expression analysis for fusion markers specific to osteoclasts such as dendritic cell-specific transmembrane protein and osteoclast stimulatory transmembrane protein.¹¹ The expression was relatively the same between the two groups (Fig. 3E). This suggests that dnMAML-expressing osteoclasts do not have a defect in gene expression required for differentiation process. However, we do expect that the fusion markers will be reduced at the protein or surface level, but this needs to be investigated further.

dnMAML Expression Suppresses Osteoclast Activity

To measure osteoclast activity, WT and dnMAML osteoclasts were differentiated and cultured on calcium phosphate coated plates and bovine cortical bone slices. In both instances, dnMAML osteoclasts demonstrated reduced resorption areas (Fig. 4A, B, E, and F). In addition, assessment of TRAP activity and C-terminal CTX-I fragments in conditioned media revealed that dnMAML osteoclasts secreted lower amounts of TRAP and digested less collagen than their WT counterparts (Fig. 4C and D).

dnMAML Suppresses Osteoclast Activity Without Impacting TRAP⁺ Cell Number or Gene Expression In Vivo

As measured by serum CTX-I ELISA, dnMAML mice (3-month old males and females) demonstrated reduced osteoclast activity compared with WT (Fig. 5A). To assess whether this effect was a result of decreased osteoclast number, TRAP staining was performed. Histomorphometric analysis of TRAP-stained sections

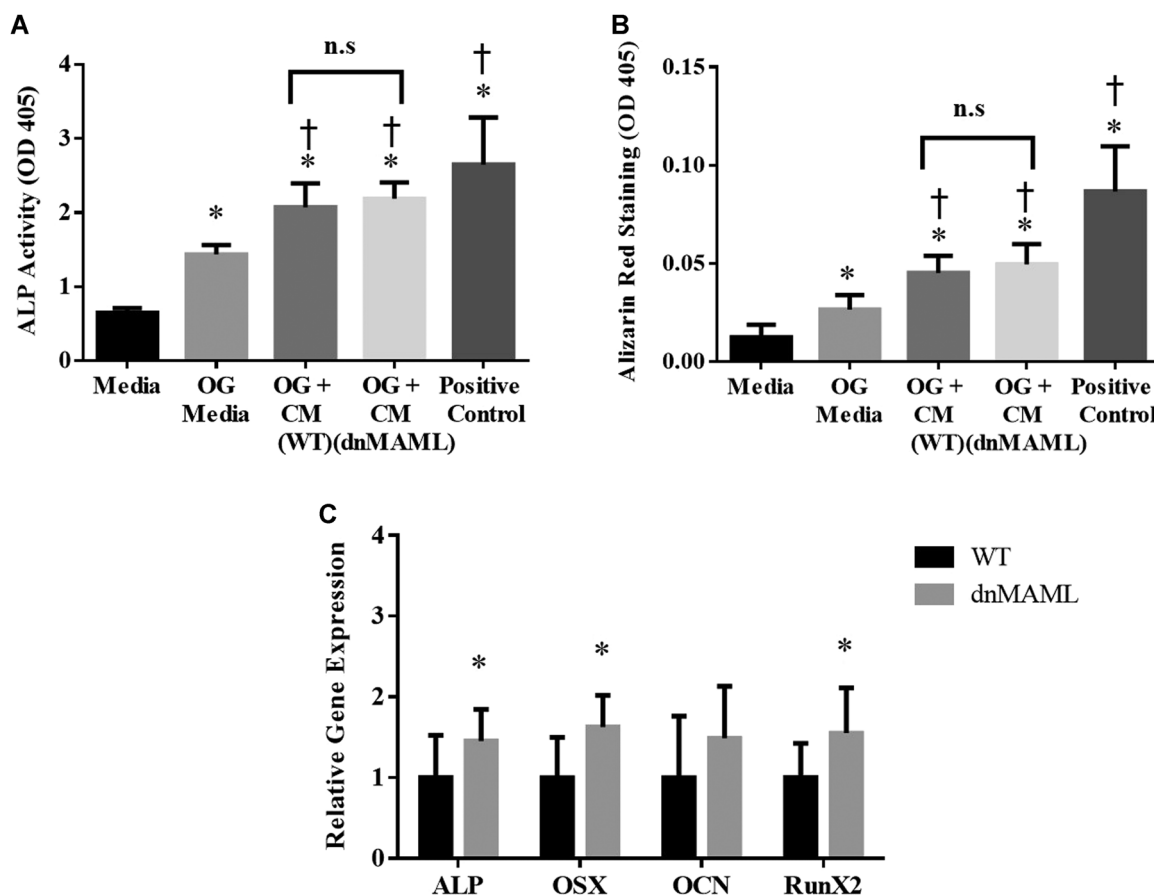


Figure 6. dnMAML osteoclasts stimulate osteogenesis. Osteoclast and osteoblast precursors were obtained from bone marrow of wild-type (WT) and dnMAML mice. Osteoblast precursors were cultured in the presence of maintenance media, osteogenic (OG) media (maintenance media supplemented with β -glycerol phosphate, ascorbate, and dexamethasone), OG media was combined with conditioned media from WT or dnMAML osteoclasts, or OG media supplemented with bone morphogenetic protein 6 (BMP-6) as a positive control. After 15 days of differentiation, (A) Alkaline phosphatase (ALP) activity was determined using SensoLyte pNPP Alkaline Phosphatase Assay Kit, and (B) calcium deposits were quantified after alizarin red staining. Both ALP activity and Alizarin Red staining were significantly increased in all treatment groups compared with maintenance media ($*p < 0.05$). Similarly, ALP activity and Alizarin Red staining were significantly increased when OG medium was supplemented with conditioned medium from both WT and dnMAML osteoclasts as well as with BMP-6 ($†p < 0.05$). There was no significant difference between cells treated with WT and dnMAML conditioned media. (C) Osteoblast genes (ALP, OSX, and RunX2) in 6-month dnMAML females were significantly increased as measured by quantitative reverse transcription polymerase chain reaction (qRT-PCR). Values represented are mean \pm SD and p value was calculated using Student t test ($*p < 0.05$, $†p < 0.05$).

and gene expression analysis in whole bone RNA revealed no significant differences in osteoclastic gene expression or TRAP⁺ cells regardless of sex (Fig. 5B and C). This suggests that, as observed *ex vivo*, dnMAML reduces osteoclast activity by keeping osteoclasts in an immature, mononuclear state.

Osteoblast Coupling to Osteoclasts is Maintained in the Absence of Osteoclast Notch Signaling

Osteoblast precursors from WT mice were cultured in presence of condition media obtained from either WT or dnMAML osteoclasts or BMP-6 as a positive control. Both ALP activity and mineralization were enhanced by treatment with osteoclast-conditioned media regardless of whether the media came from WT or dnMAML osteoclasts (Fig. 6A and B). This indicates that osteoclasts from dnMAML-expressing precursors do not lose their ability to stimulate osteoblasts even though they are

deficient in resorptive functionality. However, we cannot rule out the fact that the condition media might have some contribution from monocytes in addition to osteoclasts serving as a limiting factor for data represented in Figure 6A and B. These observations were further evidenced *in vivo* where osteoblast gene expression was found to be higher in 6-month female dnMAML mice and suggesting that inhibition of Notch pathway in osteoclasts does not negatively affect osteoblasts (Fig. 6C; Supplementary Fig. S2).

LysM-dnMAML Mice Have Increased Osteoblast Activity and Bone Strength, But Normal Bone Architecture

Mice were analyzed for morphology of key skeletal elements and bone architecture using μ CT and later tested mechanically using 3-point bending. No changes were observed in any of the parameter evaluated using μ CT (Supplementary Figs. S3A–S6A

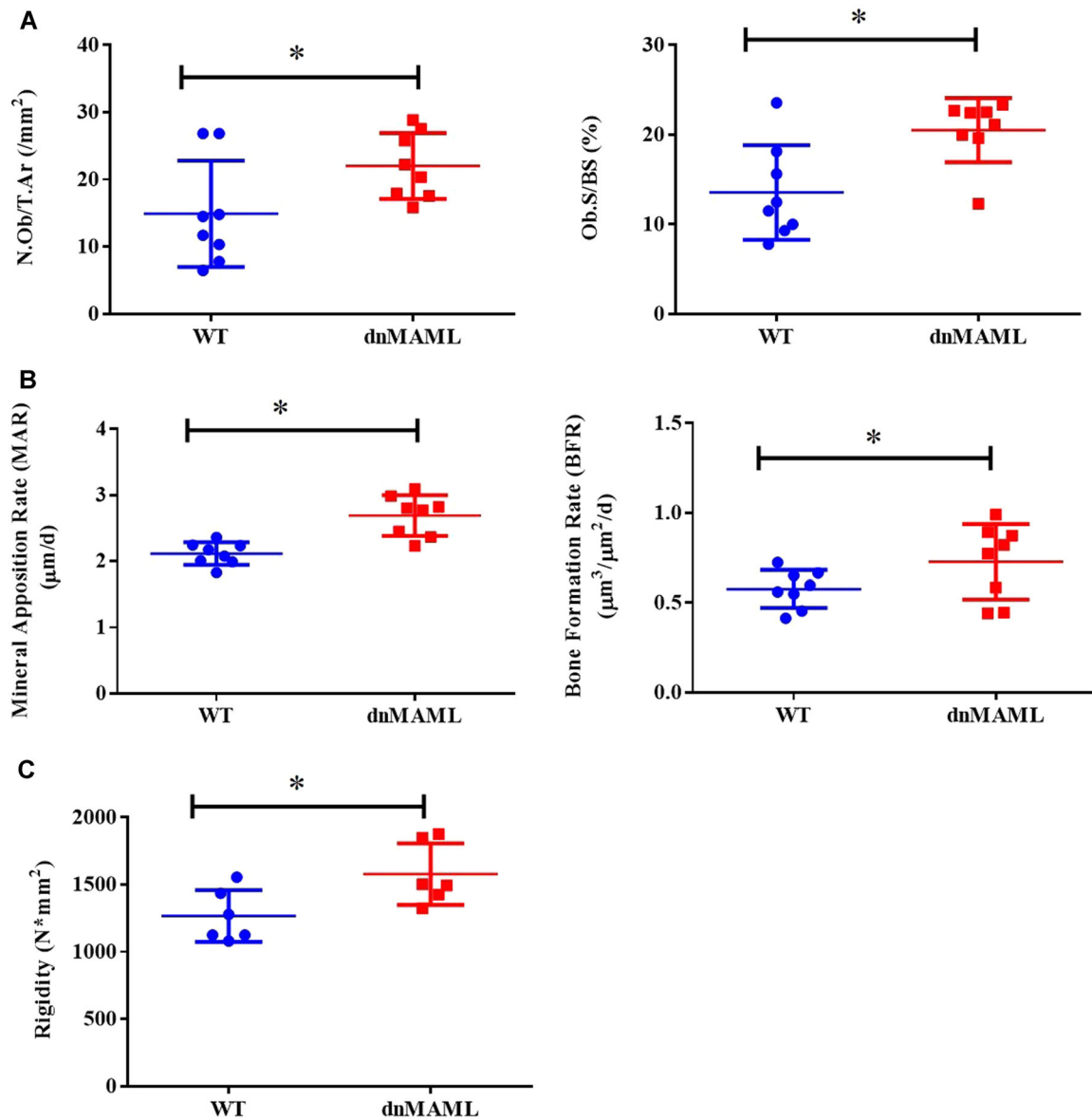


Figure 7. dnMAML mice demonstrate increased bone formation rates and bone rigidity. Wild-type (WT) and dnMAML mice were given injections of alizarin red and calcein, 8 and 1 days prior to sacrifice, respectively, to label bone mineralizing surfaces. Static and dynamic histomorphometric analyses were later performed on plastic-embedded femur sections. (A) Plastic sections were trichrome-stained, imaged, and analyzed. There was a significant increase in osteoblast number/trabecular area and osteoblast surface per bone surface percentage in dnMAML mice. (B) Dynamic histomorphometry using fluorescence microscopy on unstained sections showed significantly higher mineral apposition and bone formation rates in dnMAML group. Representative data for 6-month females are depicted. (C) Mechanical testing using 3-point bending demonstrated bones from dnMAML mice of 6-month males exhibited significantly higher rigidity. Values represented are mean \pm SD and p value was calculated using Student t test ($*p < 0.05$). [Color figure can be viewed at [wileyonlinelibrary.com](#)]

and Table S1) while there were significant changes in rigidity in 6-month male dnMAML mice (Fig. 7C; Supplementary Figs. 3B–6B and Table S1). A significantly higher number of osteoblast/trabecular area and osteoblast surface per surface were observed in 6-month females (Fig. 7A; Supplementary Figs. S7A–C and Table S2). There were also significant increases in mineral apposition rate and bone formation rate in 6-month dnMAML females (Fig. 7B, Supplementary Fig. S8A–C and Table S3). These data indicate that inhibition of osteoclast Notch signaling does not produce gross architectural changes at physiological

baseline, but, nevertheless, results in stronger bones due to increased osteoblast activity, particularly in older animals.

Inhibition of Notch Signaling in Osteoclasts Results in Larger Bony Calluses With Increased Mineral Density Following Traumatic Fracture

We observed that both 3-month-old male and female dnMAML mice showed significant improvements in fracture healing. These mice displayed significantly higher bone volume, tissue mineral, and bone mineral densities, respectively, at 40 DPF ($p < 0.05$) while no differences were

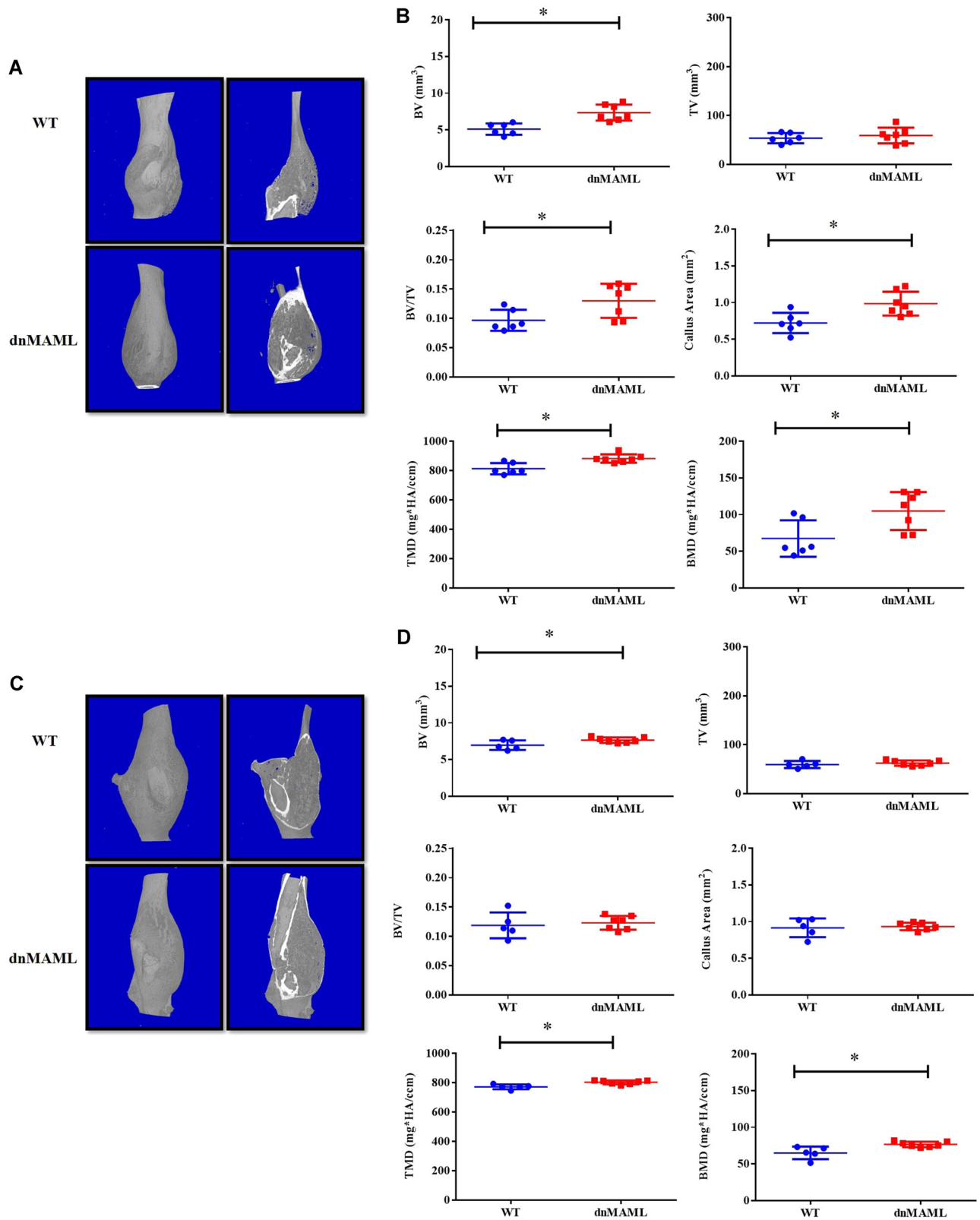


Figure 8. Inhibition of Notch signaling in osteoclasts results in larger bony calluses during fracture healing. Both 3-month-old male and female mice at 40 days post fracture (DPF) showed significantly larger bony calluses. (A) Three-dimensional (3D) images and sectional cut views obtained from μ CT in 3-month males showed (B) significant increases in bone volume, bone volume/total volume, callus area, tissue mineral density, and bone mineral density. (C) In 3-month females, there were (D) significant increases in bone volume, tissue mineral density, and bone mineral density. Values represented are mean \pm SD and p value was calculated using Student t test ($*p < 0.05$). [Color figure can be viewed at wileyonlinelibrary.com]

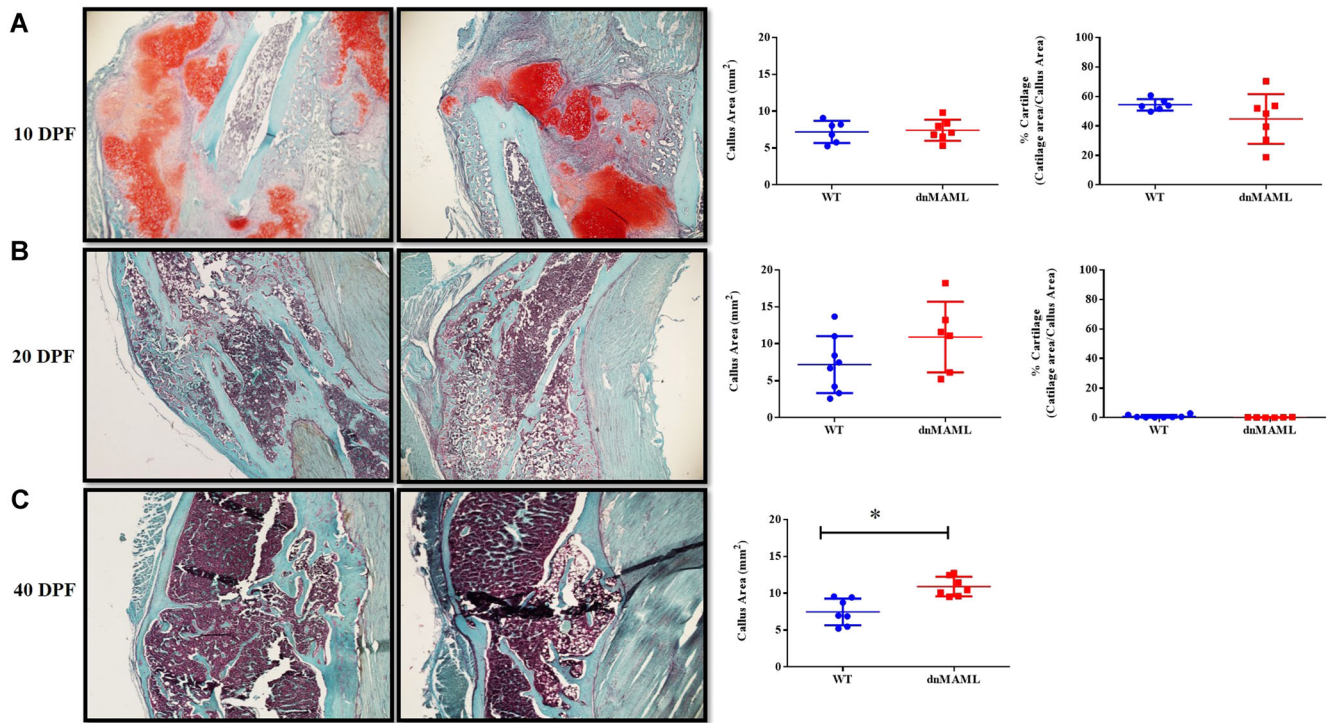


Figure 9. Inhibition of Notch signaling results in larger bony callus areas without impacting soft callus formation. Fracture calluses in 3-month males were Safranin O stained to quantify callus and cartilage areas. Following staining, cartilage-containing areas are orange/red, nuclei are black, and background bone and muscle are blue/green. Representative images at (A) 10 days post fracture (DPF) and (B) 20 DPF showed no significant difference in callus or cartilage area between wild-type (WT) and dnMAML. (C) Callus area was significantly higher in dnMAML samples at 40 DPF, at which point, no cartilage was visible in either group. Images were captured using a Nikon Eclipse light microscope at $\times 20$ magnification and were analyzed using Osteomeasure software. Values represented are mean \pm SD and *p* value was calculated using Student *t* test ($*p < 0.05$). [Color figure can be viewed at wileyonlinelibrary.com]

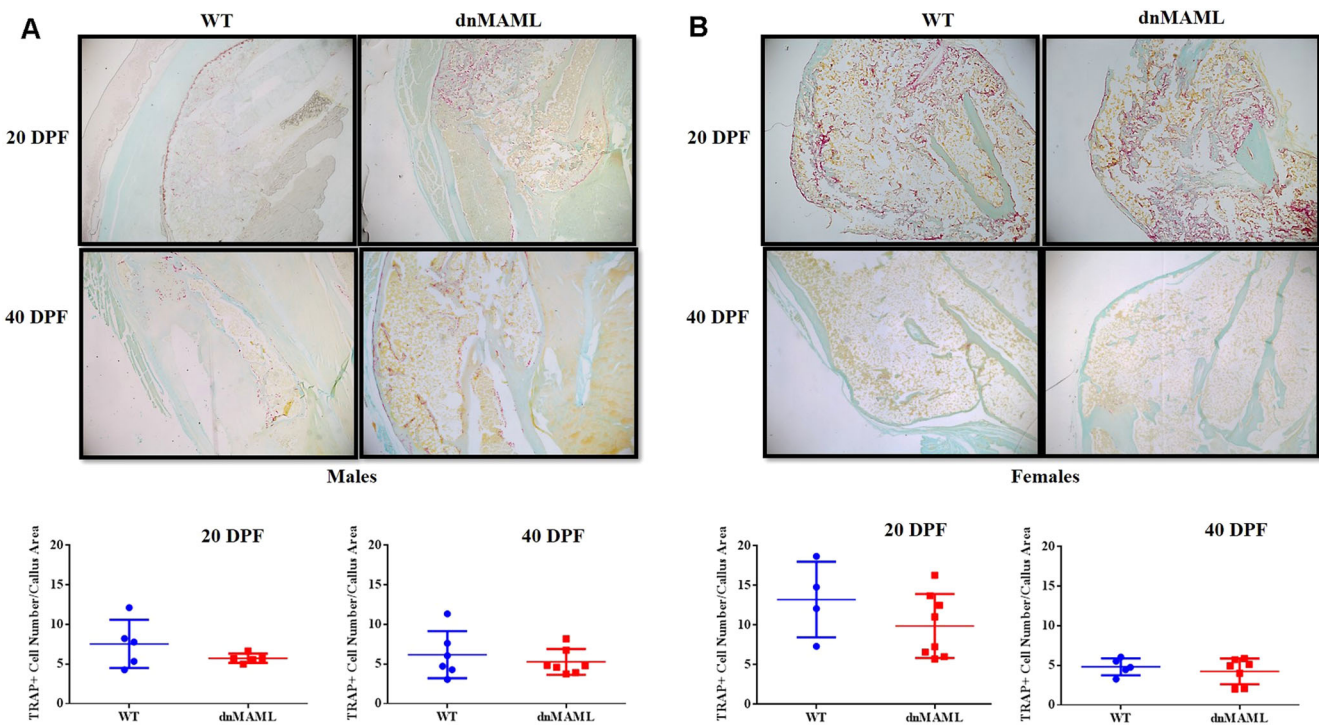


Figure 10. Notch inhibition does not impact tartrate-resistant acid phosphatase (TRAP)⁺ cell number in fracture calluses. Fracture calluses from male and female 3-month-old wild-type (WT) and dnMAML mice were TRAP-stained to evaluate the TRAP⁺ cell numbers. No differences in TRAP⁺ cell number/callus area were observed in either 20 DPF or 40 days post fracture (DPF) samples from (A) 3-month males and (B) 3-month females, respectively. Images were captured using a Nikon Eclipse light microscope at $\times 20$ magnification and were analyzed using Osteomeasure software. [Color figure can be viewed at wileyonlinelibrary.com]

observed at prior time points (Fig. 8A-D, Supplementary Fig. S9A-C and Table S4). We also observed significantly higher callus area in 40 DPF 3-month males but not females. To further corroborate these findings, histology was performed using paraffin-embedded samples. There was a significant increase in callus area in 40 DPF group ($p < 0.05$) for the males but not for female group (Fig. 9, Supplementary Fig. S10 and Table S4) while no differences in osteoclasts numbers/callus area were observed in TRAP-stained sections (Fig. 10). This indicates that Notch inhibition in osteoclasts does not affect their cellular number but, rather, their function.

DISCUSSION

Inhibition of Notch signaling or the genes it regulates in osteoclasts may be a viable method for reducing bone resorption while maintaining bone formation. Systemic inhibition of Notch signaling through global, inducible expression of dnMAML produces a net inhibitory effect on fracture healing due to the deleterious effects of dnMAML expression on bone formation.⁵⁰ Here, we investigated the effects of Notch signaling inhibition in osteoclast precursors on resting bone characteristics and the fracture healing process in vivo. Congruent with prior studies, we found that Notch inhibition via dnMAML suppressed osteoclast function both in vitro and in vivo without significant reduction of early osteoclastic gene expression or coupled osteoblast activity. From our ex vivo experiments, we hypothesize that dnMAML-expressing osteoclast precursors undergo early differentiation toward osteoclasts but fail to fuse and persist as mononuclear TRAP⁺ cells, though this morphological difference is difficult to ascertain in vivo. Furthermore, where alterations in osteoblast number or function were observed, these parameters were increased, and this resulted in increased bone formation rate and strength. With this increased osteoblast activity, however, we did not observe any significant alterations in bone architecture, which suggests that, while dnMAML-expressing osteoclasts have reduced activity, their resorptive function is sufficient for physiological bone remodeling.

Despite modest changes at physiological baseline, LysM-dnMAML mice showed significant increases in bony callus and mineralization compared with WT. Unaltered TRAP⁺ cell numbers in the healing fractures suggests that, as with uninjured animals, the increase in bone is more likely due to reduced resorptive activity rather than cell number. Taken with the physiological remodeling data, our work suggests that osteoclast Notch signaling is dispensable with respect to level of osteoclast activity required for normal remodeling. Thus, therapeutic inhibition of osteoclast Notch signaling could result in reduction of osteoclast activity in regions of the skeleton where that activity would have been pathologically elevated while sparing restorative remodeling elsewhere.

While previous clinical studies utilizing bisphosphonates and RANKL inhibition⁵¹⁻⁵³ suggested that

osteoclast inhibition does not significantly impact fracture callus parameters, the conclusions of these studies cannot distinguish between osteoclast function and osteoclast number as both interventions reduce osteoclast number by either triggering osteoclast apoptosis (bisphosphonates) or inhibiting osteoclastogenesis from an early stage (RANKL inhibition). The negative findings of these studies may be due to a concomitant decrease in osteoblast activity following reduction in osteoclast number, which would effectively neutralize any positive effect that osteoclast inhibition might have had on callus size and mineralization. Thus, while reduction of osteoclast number can promote increased bone mass and decreased fracture risk in the short term, long-term suppression of bone remodeling is a source of concern.^{54,55} Reduction of osteoclast activity without impacting their coupling to osteoblasts, as we have demonstrated with osteoclast-specific inhibition of Notch signaling, has the potential to alleviate concerns regarding long-term anti-resorptive therapy and produce larger, potentially more stable fracture calluses through the preservation of osteoclast-stimulated osteogenesis in the context of reduced bone resorption.

AUTHORS' CONTRIBUTION

JWA, JA, KDH, and PNG. designed the experiments. PNG, YM, JHB, AJE, and GK. performed the experiments. PNG, JWAs, and JA. drafted the manuscript. All the authors analyzed the data, reviewed, edited, and approved the final manuscript.

ACKNOWLEDGMENTS

We thank the AO Foundation (J.W.A.) (Project number for the AO grant is S-16-12A), NIH/NIAMS P30AR069619, and support from Department of Orthopedic Surgery, Perelman School of Medicine at the University of Pennsylvania, and Corporal Michael J. Crescenz VA Medical Center. We also thank Sarah Teegarden, Ph.D. and Garret FitzGerald, MD of the University of Pennsylvania for providing us with Lysozyme M-Cre mice. J.A. and K.D.H. are co-owners of Skelegen, a biologics company.

REFERENCES

1. Bahney CS, Zondervan RL, Allison Pet et al. 2019. Cellular biology of fracture healing. *J Orthop Res* 37:35-50.
2. Schell H, Lienau J, Epari DRet et al. 2006. Osteoclastic activity begins early and increases over the course of bone healing. *Bone* 38:547-554.
3. Takeyama K, Chatani M, Takano Yet et al. 2014. In-vivo imaging of the fracture healing in medaka revealed two types of osteoclasts before and after the callus formation by osteoblasts. *Dev Biol* 394:292-304.
4. Beraldi R, Masi L, Parri Set al. 2014. The role of the orthopaedic surgeon in the prevention of refracture in patients treated surgically for fragility hip and vertebral fracture. *Clin Cases Miner Bone Metab* 11:31-35.
5. Hobby B, Lee MA. 2013. Managing atrophic nonunion in the geriatric population: incidence, distribution, and causes. *Orthop Clin North Am* 44:251-256.

6. Sibai T, Morgan EF, Einhorn TA. 2011. Anabolic agents and bone quality. *Clin Orthop Relat Res* 469:2215–2224.
7. Dimitriou R, Jones E, McGonagle Det al. 2011. Bone regeneration: current concepts and future directions. *BMC Med* 9:66.
8. Giannotti S, Bottai V, Dell'osso Get al. 2013. Current medical treatment strategies concerning fracture healing. *Clin Cases Miner Bone Metab* 10:116–120.
9. Kostenuik P, Mirza FM. 2017. Fracture healing physiology and the quest for therapies for delayed healing and nonunion. *J Orthop Res* 35:213–223.
10. Levaot N, Ottolenghi A, Mann Met al. 2015. Osteoclast fusion is initiated by a small subset of RANKL-stimulated monocyte progenitors, which can fuse to RANKL-unstimulated progenitors. *Bone* 79:21–28.
11. Soe K, Hobolt-Pedersen AS, Delaisse JM. 2015. The elementary fusion modalities of osteoclasts. *Bone* 73:181–189.
12. Henriksen K, Karsdal MA, Martin TJ. 2014. Osteoclast-derived coupling factors in bone remodeling. *Calcified Tissue Int* 94:88–97.
13. Karsdal MA, Martin TJ, Bollerslev Jet al. 2007. Are nonresorbing osteoclasts sources of bone anabolic activity? *J Bone Miner Res* 22:487–494.
14. Ota K, Quint P, Ruan Met al. 2013. TGF-beta induces Wnt10b in osteoclasts from female mice to enhance coupling to osteoblasts. *Endocrinology* 154:3745–3752.
15. Pederson L, Ruan M, Westendorf JJet al. 2008. Regulation of bone formation by osteoclasts involves Wnt/BMP signaling and the chemokine sphingosine-1-phosphate. *Proc Natl Acad Sci USA* 105:20764–20769.
16. Teitelbaum SL. 2016. Therapeutic implications of suppressing osteoclast formation versus function. *Rheumatology (Oxford)* 55:ii61–ii63.
17. Bai S, Kopan R, Zou Wet al. 2008. NOTCH1 regulates osteoclastogenesis directly in osteoclast precursors and indirectly via osteoblast lineage cells. *J Biol Chem* 283:6509–6518.
18. Fukushima H, Nakao A, Okamoto Fet al. 2008. The association of Notch2 and NF-kappaB accelerates RANKL-induced osteoclastogenesis. *Mol Cell Biol* 28:6402–6412.
19. Sekine C, Koyanagi A, Koyama Net al. 2012. Differential regulation of osteoclastogenesis by Notch2/Delta-like 1 and Notch1/Jagged1 axes. *Arthritis Res Ther* 14:R45.
20. Yamada T, Yamazaki H, Yamane Tet al. 2003. Regulation of osteoclast development by Notch signaling directed to osteoclast precursors and through stromal cells. *Blood* 101:2227–2234.
21. Ashley JW, Ahn J, Hankenson KD. 2015. Notch signaling promotes osteoclast maturation and resorptive activity. *J Cell Biochem* 116:2598–2609.
22. Kitagawa M. 2016. Notch signalling in the nucleus: roles of Mastermind-like (MAML) transcriptional coactivators. *J Biochem* 159:287–294.
23. McElhinny AS, Li JL, Wu L. 2008. Mastermind-like transcriptional co-activators: emerging roles in regulating cross talk among multiple signaling pathways. *Oncogene* 27:5138–5147.
24. Andersson ER, Sandberg R, Lendahl U. 2011. Notch signaling: simplicity in design, versatility in function. *Development* 138:3593–3612.
25. Maillard I, Tu L, Sambandam Aet al. 2006. The requirement for Notch signaling at the beta-selection checkpoint in vivo is absolute and independent of the pre-T cell receptor. *J Exp Med* 203:2239–2245.
26. Clausen BE, Burkhardt C, Reith Wet al. 1999. Conditional gene targeting in macrophages and granulocytes using LysMcre mice. *Transgenic Res* 8:265–277.
27. Croke M, Ross FP, Korhonen Met al. 2011. Rac deletion in osteoclasts causes severe osteopetrosis. *J Cell Sci* 124:3811–3821.
28. Qi B, Cong Q, Li Pet al. 2014. Ablation of Tak1 in osteoclast progenitor leads to defects in skeletal growth and bone remodeling in mice. *Sci Rep* 4:7158.
29. Stemig M, Astelford K, Emery Aet al. 2015. Deletion of histone deacetylase 7 in osteoclasts decreases bone mass in mice by interactions with MITF. *PLoS ONE* 10:e0123843.
30. Kaur G, Ahn J, Hankenson KDet al. 2017. Stimulation of notch signaling in mouse osteoclast precursors. *J Vis Exp* 120.
31. Vesprey A, Yang W. 2016. Pit assay to measure the bone resorptive activity of bone marrow-derived osteoclasts. *Bio Protoc* 6:6.
32. Merrill DM, Pirapaharan DC, Andreasen CMet al. 2015. Pit- and trench-forming osteoclasts: a distinction that matters. *Bone Res* 3:15032.
33. Panwar P, Soe K, Guido RVet al. 2016. A novel approach to inhibit bone resorption: exosite inhibitors against cathepsin K. *Br J Pharmacol* 173:396–410.
34. Boissy P, Andersen TL, Abdallah BMet al. 2005. Resveratrol inhibits myeloma cell growth, prevents osteoclast formation, and promotes osteoblast differentiation. *Cancer Res* 65:9943–9952.
35. Soe K, Andersen TL, Hobolt-Pedersen ASet al. 2011. Involvement of human endogenous retroviral syncytin-1 in human osteoclast fusion. *Bone* 48:837–846.
36. Srivastava AK, Bhattacharyya S, Castillo Get al. 2000. Development and evaluation of C-telopeptide enzyme-linked immunoassay for measurement of bone resorption in mouse serum. *Bone* 27:529–533.
37. Greenblatt MB, Tsai JN, Wein MN. 2017. Bone turnover markers in the diagnosis and monitoring of metabolic bone disease. *Clin Chem* 63:464–474.
38. Li LJ, Kim SN, Cho SA. 2016. Comparison of alkaline phosphatase activity of MC3T3-E1 cells cultured on different Ti surfaces: modified sandblasted with large grit and acid-etched (MSLA), laser-treated, and laser and acid-treated Ti surfaces. *J Adv Prosthodont* 8:235–240.
39. Knight MN, Karuppaiah K, Lowe Met al. 2018. R-spondin-2 is a Wnt agonist that regulates osteoblast activity and bone mass. *Bone Res* 6:24.
40. Rentsch C, Schneiders W, Manthey Set al. 2014. Comprehensive histological evaluation of bone implants. *Biomater* 4:4.
41. Gruber HE. 1992. Adaptations of Goldner's Masson trichrome stain for the study of undecalcified plastic embedded bone. *Biotech Histochem* 67:30–34.
42. Zondervan RL, Vorce M, Servadio N. 2018. Fracture apparatus design and protocol optimization for closed-stabilized fractures in Rodents. *J Vis Exp* 138.
43. Bouxsein ML, Boyd SK, Christiansen BAet al. 2010. Guidelines for assessment of bone microstructure in rodents using micro-computed tomography. *J Bone Miner Res* 25:1468–1486.
44. de Bakker CM, Altman AR, Tseng WJet al. 2015. muCT-based, in vivo dynamic bone histomorphometry allows 3D evaluation of the early responses of bone resorption and formation to PTH and alendronate combination therapy. *Bone* 73:198–207.
45. O'Neill KR, Stutz CM, Mignemi NAet al. 2012. Micro-computed tomography assessment of the progression of fracture healing in mice. *Bone* 50:1357–1367.
46. Morgan EF, Mason ZD, Chien KBet al. 2009. Micro-computed tomography assessment of fracture healing: relationships among callus structure, composition, and mechanical function. *Bone* 44:335–344.

47. Kahveci Z, Minbay FZ, Cavusoglu L. 2000. Safranin O staining using a microwave oven. *Biotech Histochem* 75:264–268.
48. Tran D, Golick M, Rabinovitz H et al. 2000. Hematoxylin and safranin O staining of frozen sections. *Dermatol Surg* 26: 197–199.
49. Camplejohn KL, Allard SA. 1988. Limitations of safranin “O” staining in proteoglycan-depleted cartilage demonstrated with monoclonal antibodies. *Histochemistry* 89:185–188.
50. Dishowitz MI, Mutyaba PL, Takacs JDet et al. 2013. Systemic inhibition of canonical Notch signaling results in sustained callus inflammation and alters multiple phases of fracture healing. *PLoS ONE* 8:e68726.
51. Delos D, Yang X, Ricciardi BF et al. 2008. The effects of RANKL inhibition on fracture healing and bone strength in a mouse model of osteogenesis imperfecta. *J Orthop Res* 26: 153–164.
52. Kates SL, Ackert-Bicknell CL. 2016. How do bisphosphonates affect fracture healing? *Injury* 47:S65–S68.
53. Xue D, Li F, Chen G et al. 2014. Do bisphosphonates affect bone healing? A meta-analysis of randomized controlled trials. *J Orthop Surg Res* 9:45.
54. Rasmusson L, Abtahi J. 2014. Bisphosphonate associated osteonecrosis of the jaw: an update on pathophysiology, risk factors, and treatment. *Int J Dent* 2014:471035–471039.
55. Sellmeyer DE. 2010. Atypical fractures as a potential complication of long-term bisphosphonate therapy. *JAMA* 304:1480–1484.

SUPPORTING INFORMATION

Additional supporting information may be found in the online version of this article.